Thiazole-linked isomeric covalent organic frameworks for divergent photocatalysis: Selective oxidation of organic sulfides

Yuexin Wang [a], Fulin Zhang [a], Fengwei Huang [a], Xiaoyun Dong [a], Bing Zeng [a], Xiang-Kui Gu [b], Xianjun Lang [a,*]

[a] Hubei Key Lab on Organic and Polymeric Optoelectronic Materials, College of Chemistry and Molecular Sciences, Wuhan University, Wuhan 430072, China
[b] School of Power and Mechanical Engineering, Wuhan University, Wuhan 430072, China

ARTICLE INFO

ABSTRACT

The photocatalysis of covalent organic frameworks (COFs) is underpinned by their inherent structures in which the linkage plays a vital role in determining the activity. The transformation of imine into thiazole leads to isomeric structures owing to the different orientations of linkages. Here, two thiazole-linked COFs, COF-TZ-1 and COF-TZ-2, are constructed from two imine-linked COFs, COF-IM-1 and COF-IM-2, with the imine N next to the linker triphenylbenzene and triphenyltriazine, respectively. Despite better absorption, COF-TZ-1 possesses inferior optoelectronic properties to COF-TZ-2. Besides, the dipole moment of COF-TZ-2 is twice that of COF-TZ-1. COF-TZ-2 is much better than COF-TZ-1 for blue light photocatalytic selective oxidation of organic sulfides with O_2 under blue light irradiation. Furthermore, the facile adsorption sites of O_2 are verified by density functional theory calculations, and the generation of superoxide is tracked over COF-TZ-2. This work highlights that subtle variations of COFs can lead to divergent photocatalysis.

1. Introduction

Two-dimensional (2D) covalent organic frameworks (COFs) with extended π-conjugated planes of organic groups have been meticulously exploited for energy and environmental applications [1–4]. Their structural tunability can afford the desired properties like broadened absorption edges and adequate lifetime of charge carriers. Currently, various strategies for ameliorating the properties of COFs have centered on selecting photoactive building blocks for COFs [5–10] or controlling the construction conditions [11–14]. Notably, early research has verified that isomerism makes a great contribution to the different properties of COFs [15–18]. Besides, isomeric COFs can accurately reflect the relationship between the structure and property of COFs. In this context, tuning the interlayer stacking [19] and altering the topological structure [20–22] are accessible to explore the structure–activity relationship of isomeric COFs, which can be realized through selecting building blocks with different conformation [23]. Furthermore, COFs with position isomerism are generally constructed with isomeric building blocks [24–26] or differently functionalized building blocks [27].

Presumably, the different orientations of the linkage constructed under the same condensation conditions can be exploited to result in isomeric COFs. Importantly, the subtle alteration affected by different orientations of linkages also exhibits substantial differences in opto-electronic properties and consequent photocatalytic activities [28–30]. Thereinto, the structure–activity relationship between the C═N linkage with different orientations within COFs has been established with different properties [31–33]. Even so, based on the feasibility of COFs, exploring the structure–activity relationship through linkages other than imine with different orientations remains much more challenging. Therefore, other linkages should be applied to consider the structure-e–activity relationship of COFs. As such, thiazole group, a promising linkage with intrinsic photoactive activity, has been exploited into COFs [34–36]. It is indispensable to consider the influence of different orientations of thiazole linkages in isomeric COFs on photocatalytic activity. In particular, the intrinsic stability and permanent porosity endow COFs with enormous advantages in selective organic transformations [37–43].

Herein, incorporating triphenylbenzene and triphenyltriazine as the linkers, owing to the difference in the orientation of imine and thiazole linkages, two imine-linked isomeric COFs and two thiazole-linked isomeric COFs are constructed successfully. Particularly, based on a typical aldimine condensation, triphenylbenzene and triphenyltriazine

---

* Corresponding author.
 E-mail address: xianjunlang@whu.edu.cn (X. Lang).

are installed with three aldehyde and amine groups or vice versa, affording two imine-linked isomeric COFs, COF-IM-1 and COF-IM-2. Moreover, the imine linkages are converted into the thiazole linkages through cascade cycloaddition with sulfur, affording COF-TZ-1 and COF-TZ-2 (Fig. 1). To explore the structure–activity relationship, the optoelectronic properties of the four COFs are probed by experiments and theoretical calculations. Intriguingly, the presence of electron deficient benzothiazole next to triazine contributes to a larger dipole moment, which endows COF-TZ-2 with superior charge separation and in-plane electron transfer. Hence, the photocatalytic activity of COF-TZ-2 is superior to COF-TZ-1 for selective oxidation of organic sulfides with O_2 under blue LED (light-emitting diode) irradiation. This work highlights the structure–activity relationship between the linkage of different orientations and the divergent photocatalytic activity over 2D COFs.

2. Experimental section

2.1. Reagents and solvents

The 1,3,5-tris(4-aminophenyl)benzene, 1,3,5-tris(4-formylphenyl)triazine, 1,3,5-tris(4-aminophenyl)triazine, 1,3,5-tris(4-formylphenyl)benzene, 1,4-dioxane, mesitylene, and *o*-dichlorobenzene were purchased from Adamas. The anhydrous *n*-butyl alcohol was produced by Thermos Scientific. Toluene, acetic acid, sublimed sulfur (S_8) powder, and tetrahydrofuran (THF) were obtained from Sinopharm Chemical Reagent.

2.2. The construction of COF-IM-1, COF-IM-2, COF-TZ-1, and COF-TZ-2

COF-IM-1 and COF-IM-2 were constructed through solvothermal condensations in line with a previous report [28]. Detailly, for COF-IM-1, in a 10 mL Pyrex tube, 0.05 mmol 1,3,5-tris(4-aminophenyl) benzene, 0.05 mmol 1,3,5-tris(4-formylphenyl)triazine, and 0.1 mL 6 M acetic acid aqueous solution were dispersed in 1 mL mixed solvent of 1, 4-dioxane and mesitylene (1:1). Besides, for COF-IM-2, in a 20 mL Pyrex tube, 0.15 mmol 1,3,5-tris(4-aminophenyl)triazine, 0.15 mmol 1,3, 5-tris(4-formylphenyl)benzene, and 0.4 mL 6 M acetic acid aqueous solution were dispersed in 4 mL mixed solvent of *o*-dichlorobenzene and *n*-butyl alcohol (1:1). Commonly, degassed through three freeze–pump–thaw cycles, under vacuum, the Pyrex tube was flame-sealed. Finally, the Pyrex tube with the mixture was heated for 72 h at 120 °C. The yellow precipitate obtained was purified by Soxhlet extraction with THF and desiccated under vacuum for 12 h at 120 °C.

COF-TZ-1 and COF-TZ-2 were constructed through post-synthetic modifications referring to a reported procedure with some modifications [44]. COF-IM-1 was activated at 150 °C for 12 h, and the activated COF-IM-1 was mixed and ground adequately with excess S_8 (15-fold weight amount). Next, the mixture was heated under flowing argon in the tubular furnace: 60 °C (1 h), 155 °C (3 h), and 350 °C (3 h) in sequence. The obtained powder was rinsed with toluene and purified by Soxhlet extraction with THF. At last, the excess solvent and S_8 were removed through heating at 150 °C under vacuum to afford COF-TZ-1. COF-TZ-2 was constructed in a similar procedure to that of COF-TZ-1.
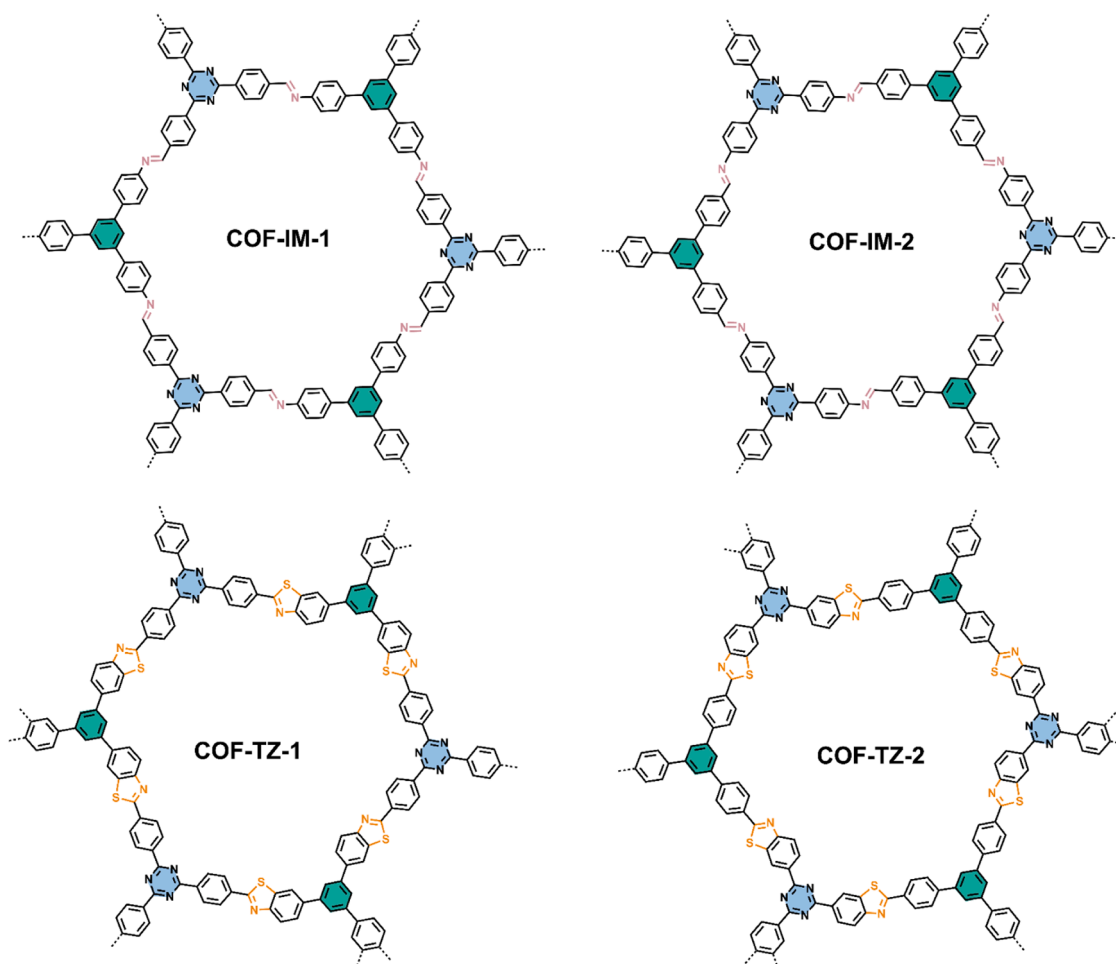

Fig. 1. The chemical backbones of the imine-linked isomeric COFs of COF-IM-1 and COF-IM-2 and the thiazole-linked isomeric COFs of COF-TZ-1 and COF-TZ-2.

3. Results and discussion

3.1. Characterizations and activity of the imine- and thiazole-linked isomeric COFs

COF-IM-1 and COF-IM-2 were constructed through the traditional solvothermal condition with the condensation of 1,3,5-tris(4-aminophenyl)benzene with 1,3,5-tris(4-formylphenyl)triazine and the condensation of 1,3,5-tris(4-aminophenyl)triazine with 1,3,5-tris(4-formylphenyl)benzene. Furthermore, the reversible imine linkages were converted into the thiazole linkages by cascade cycloaddition with S_8, affording two thiazole-linked isomeric COFs, COF-TZ-1 and COF-TZ-2. Fig. 1 delineates the chemical backbones of COF-IM-1, COF-IM-2, COF-TZ-1, and COF-TZ-2. Fig. 2 illustrates the high crystallinity of COF-TZ-1, COF-IM-1, COF-TZ-2, and COF-IM-2 through powder X-ray diffraction (PXRD) patterns. Thereinto, a visible diffraction peak at a low angle was assigned to (100) reflection, $2\theta = 4.04°$ for COF-TZ-1, 4.06° for COF-IM-1, 4.12° for COF-TZ-2, and 4.16° for COF-IM-2. Besides, the location and relative intensity of diffraction peaks of COF-IM-1 and COF-IM-2 correspond well with the previous reports [13,45]. With resembled structures, the PXRD patterns of COF-TZ-1 and COF-TZ-2 are similar to those of COF-IM-1 and COF-IM-2, respectively. Additionally, the weak diffraction peaks around 7.10° and 8.20° corresponded to the (110) and (200) crystal planes, respectively. The change of relative intensities of

(110) and (200) reflections was attributed to the deformation of hexagonal pores caused by the formation of benzothiazole. The simulated PXRD patterns of AA stackings of COF-TZ-1, COF-IM-1, COF-TZ-2, and COF-IM-2 are also presented in Fig. 2. Compared with the simulated results, the PXRD results are in agreement with AA stacking. The conversions of imine-linked isomeric COFs, COF-IM-1 and COF-IM-2, into thiazole-linked isomeric COFs, COF-TZ-1 and COF-TZ-2, reserved the high crystallinity and AA stacking.

The successful constructions of COF-TZ-1, COF-IM-1, COF-TZ-2, and COF-IM-2 were verified through the appearance of characteristic vibrations of C=N in Fourier-transform infrared (FTIR) spectra. As unveiled in Figure S1, the obvious decline in the peak at 1690–1697 cm^{-1} (C=O stretching vibration) and the appearance of the peak at 1621 cm^{-1} in COF-IM-1 and 1625 cm^{-1} in COF-IM-2 (C=N stretching vibration) manifest the occurrence of aldimine condensation of the building blocks [13]. Different from COF-IM-1, the peak of C=N stretching vibration in COF-TZ-1 appeared at 1601 cm^{-1} (Fig. 3a), which is attributed to the shift of the electron cloud of N in the thiazole linkage. Also, the peak of C=N stretching vibration shifted from 1625 cm^{-1} in COF-IM-2 to 1599 cm^{-1} in COF-TZ-2 (Fig. 3b), suggesting the successful conversion of the imine-linked isomeric COFs into the thiazole-linked isomeric COFs. Besides, the peaks at 970 cm^{-1} in COF-TZ-1 and 971 cm^{-1} in COF-TZ-2 are attributed to the stretching modes of the thiazole linkage.
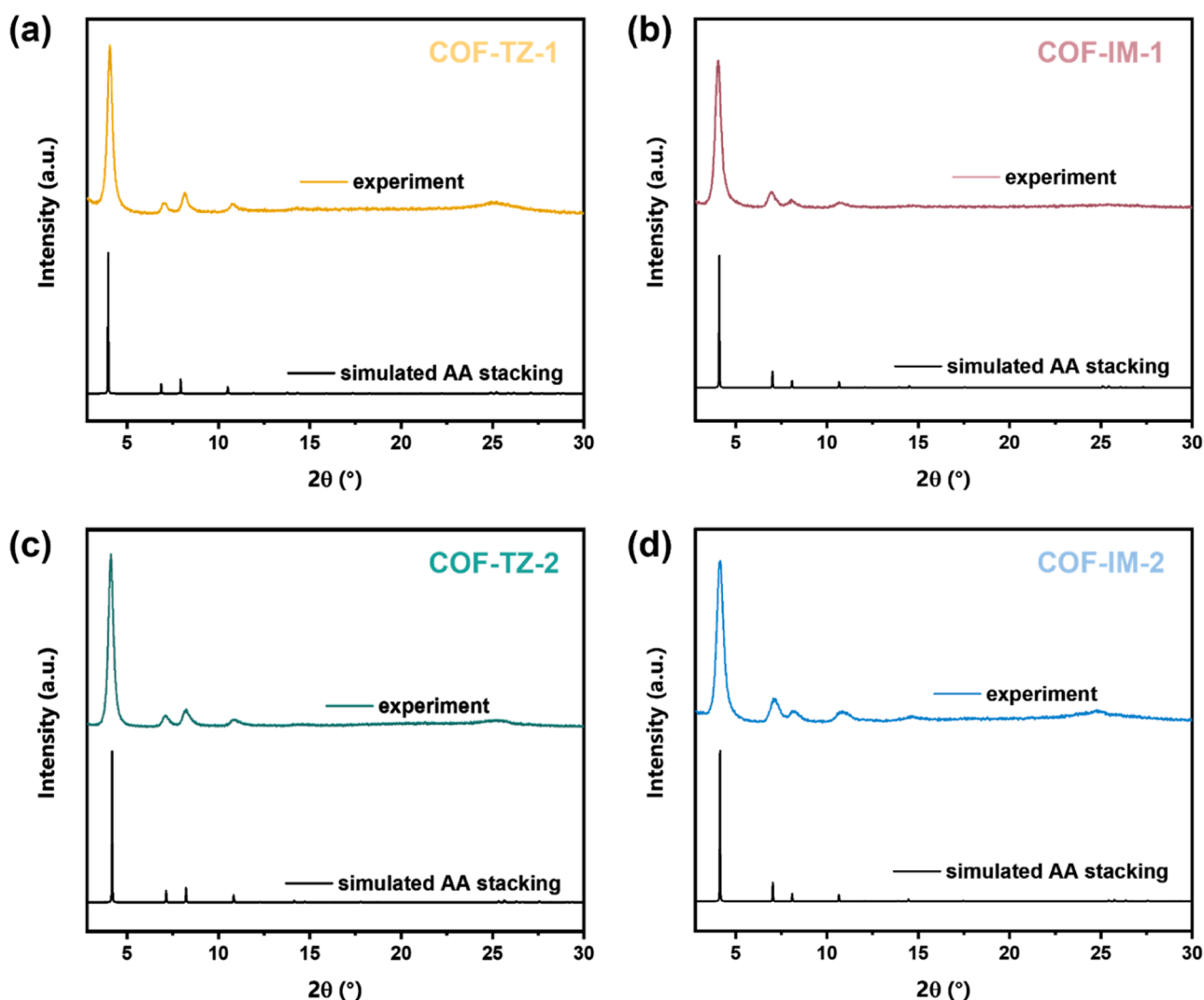

Fig. 2. The experimental and simulated PXRD patterns of COF-TZ-1 (a); COF-IM-1 (b); COF-TZ-2 (c); and COF-IM-2 (d).
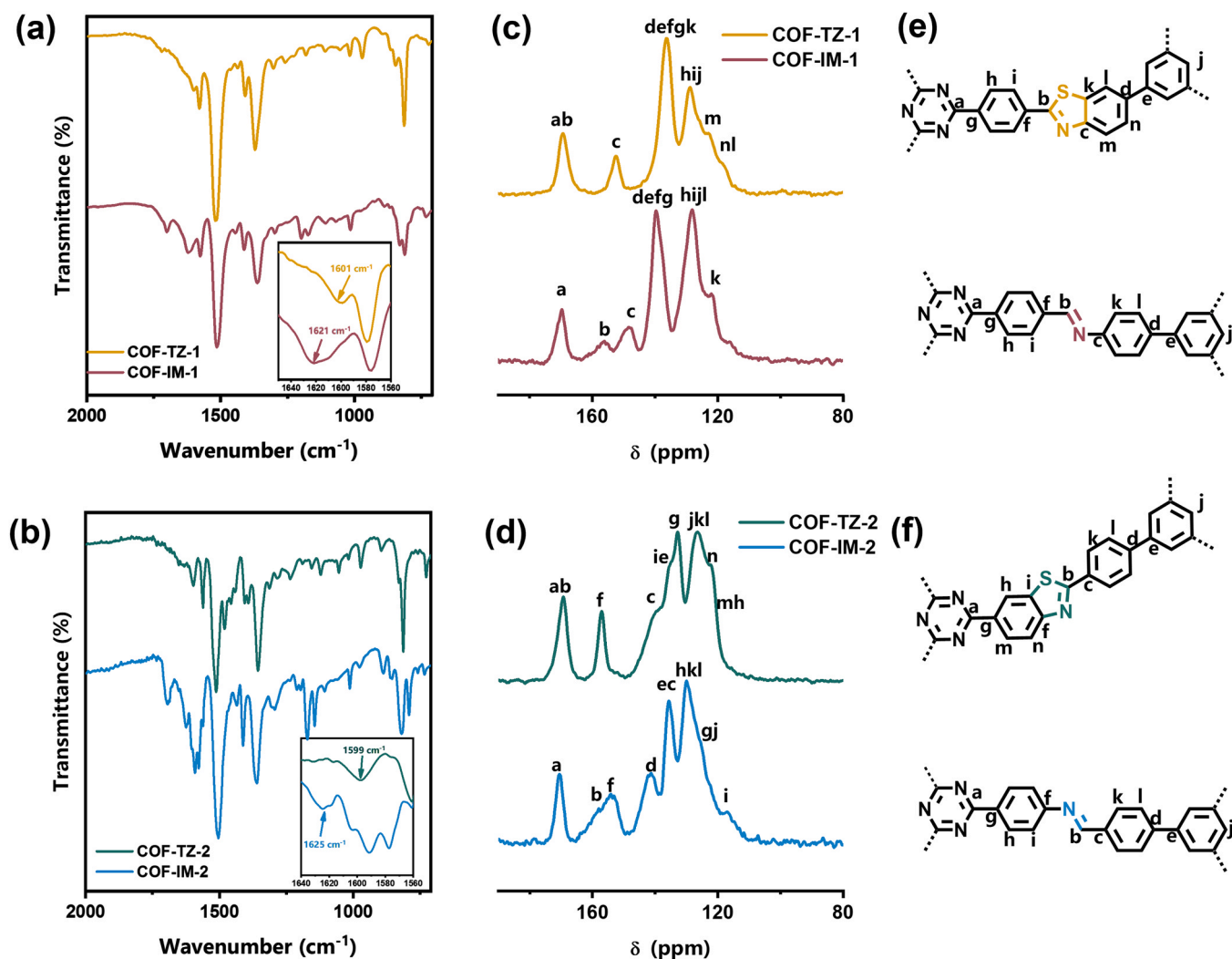
Fig. 3. FTIR spectra (a and b), solid-state ^{13}C NMR spectra (c and d), and assignment of ^{13}C signals in the corresponding molecular structures (e and f) of COF-TZ-1 (yellow line), COF-IM-1 (red line), COF-TZ-2 (green line), and COF-IM-2 (blue line).
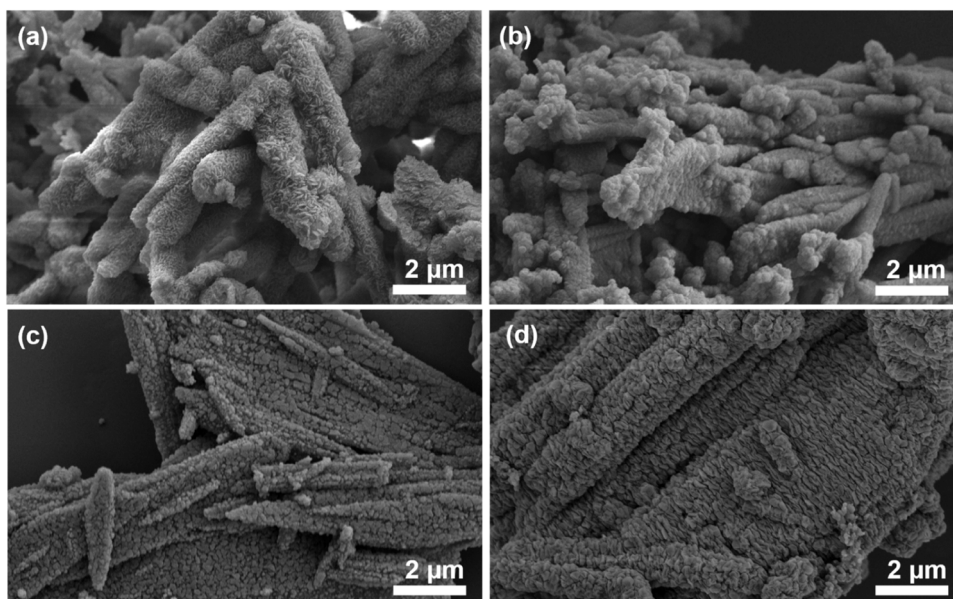

Fig. 4. The SEM images of COF-TZ-1 (a); COF-IM-1 (b); COF-TZ-2 (c); and COF-IM-2 (d).

The chemical structures of COF-TZ-1 and COF-IM-1 were further identified through the solid-state ^{13}C nuclear magnetic resonance (NMR) spectra (Fig. 3c). The disappearance of the peak at 156 ppm is attributed to isolated C≡N, and the peak of C≡N in thiazole reappeared at 170 ppm, in line with the formation of thiazole linkages. Meanwhile, the characteristic peak of C adjacent to imine-N of COF-IM-1 shifted by 4 ppm and appeared at 152 ppm, ascribed to a decrease in the electron cloud density caused by the formation of thiazole linkages. The changes in chemical shifts assigned to C in benzene and the corresponding assignments of the peaks are labeled in Fig. 3e, coinciding well with the previous work [46]. The successful construction of COF-IM-2 was also verified in Fig. 3d, corresponding well with the reported work [47]. The formation of the thiazole linkage in COF-TZ-2 was based on cascade cycloaddition of the imine linkage of COF-IM-2 with S_8. There was chemical shift of C≡N from 158 to 169 ppm and alterations of the characteristic peak of *ortho* and *meta* carbon of adjacent to benzene. Besides, comparing with the theoretical elemental content, the elemental analysis provided evidence for the incorporation of S element into COF-TZ-1 and COF-TZ-2. In general, these results sufficiently corroborate the successful construction of COF-TZ-1 and COF-TZ-2 (Table S1).

The morphologies of the four COFs were revealed through scanning electron microscopy (SEM). As exposed in Fig. 4, COF-TZ-1, COF-IM-1, COF-TZ-2, and COF-IM-2 integrally possessed agminated nanorods composed of different textural nanosheets. These can be interpreted as the consequence of the similar chemical structure. In contrast, the nanosheets of COF-IM-1 were thicker and straighter than those of COF-TZ-1 (Fig. 4a and b), and the nanosheets of COF-IM-2 were more crooked than that of COF-TZ-2 (Fig. 4c and d). Thus, the transformation of the linkage from imine to thiazole had a great impact on the textures of the COFs. Besides, elemental mapping images (Figure S2) of the four COFs illustrate the absence of S element in COF-IM-1 and COF-IM-2 and the presence of S element in COF-TZ-1 and COF-TZ-2, hinting the successful conversion of linkages from imine into thiazole. Furthermore, transmission electron microscopy (TEM) was also carried out. The lattice fringes and ordered hexagonal pores were obviously observed in the four COFs (Figure S3), corroborating that high crystallinity and ordered porous structures of COF-IM-1 and COF-IM-2 are reserved after the conversion of linkage from imine to thiazole of COF-TZ-1 and COF-TZ-2, respectively.

N_2 sorption analysis was exploited to estimate the specific surface area and porosity of COF-TZ-1, COF-IM-1, COF-TZ-2, and COF-IM-2 (Fig. 5a). The microporosities of the four COFs were assessed by the emergence of speedy increase in the isotherms at $P/P_0 < 0.1$. Besides, isotherms were analyzed with density functional theory (DFT) fitting to attain the pore size distributions for the four COFs (Figure S4). Due to the similar molecular structures, COF-TZ-1 and COF-TZ-2 exhibited approximately uniform pore size distributions. Notably, the specific surface areas for COF-TZ-1, COF-IM-1, COF-TZ-2, and COF-IM-2 were 607, 986, 957, and 628 $m^2 \ g^{-1}$, respectively.

UV–visible DRS (diffuse reflectance spectroscopy) of COF-TZ-1, COF-IM-1, COF-TZ-2, and COF-IM-2 are depicted in Fig. 5b. The absorptions of COF-TZ-1, COF-IM-1, COF-TZ-2, and COF-IM-2 were extended to range beyond 500 nm, suggesting that they can utilize of a wide range of visible light. Besides, the optical band gap (E_g) is obtained through Tauc plots. The E_g of COF-IM-1 COF-IM-2 are 2.58 and 2.70 eV, respectively. Moreover, the E_g of COF-TZ-1 and COF-TZ-2 are 2.44 and 2.60 eV, respectively. The difference in E_g implies that the alteration of the orientation of linkages has a great impact on the E_g of the COFs.

The lowest unoccupied molecular orbital (LUMO) level of a COF can be evaluated through Mott–Schottky plots. The approximate level of the LUMO is close to the flat band potential of COF. As Figure S5 elaborated, the LUMO levels of COF-TZ-1, COF-IM-1, COF-TZ-2, and COF-IM-2 were −0.85, −0.78, −0.88, and −0.80 V vs. Ag/AgCl, respectively. Therefore, the four COFs are appropriate for the reduction of O_2 to $O_2^{\bullet-}$ ($O_2/O_2^{\bullet-}$ = −0.48 V vs. Ag/AgCl). Besides, COF-TZ-1, COF-IM-1, COF-TZ-2, and COF-IM-2 belong to n-type semiconductors, inferred from the positive slopes of Mott–Schottky plots [48].

The electronic structures of the four COFs, COF-TZ-1, COF-IM-1, COF-TZ-2, and COF-IM-2, were additionally analyzed using DFT calculations. These four COFs exhibited similar band structures (Fig. 6), based on resembled molecular structures. From the charge density distributions of LUMO and the highest occupied molecular orbital (HOMO), regardless of the structures of these COFs, there was intramolecular charge migration from the central benzene of triphenylbenzene into triazine of triphenyltriazine. This charge migration is also supported by the charge density difference of LUMO to HOMO (Figure S6). Besides, the localization of HOMO in triphenylbenzene is beneficial for charge transport [49]. Based on the density of states (DOS) analysis, the S hybrid orbitals do not contribute to the variations of HOMO levels of COF-TZ-1 and COF-TZ-2 in comparsion with those of COF-IM-1 and COF-IM-2. In contrast, the S hybrid orbitals of COF-TZ-1 and COF-TZ-2 have a moderate influence on the LUMO levels of the COFs in comparsion to those of COF-IM-1 and COF-IM-2. Intriguingly, benzothiazole as an electron-withdrawing group alters, to some degree, the charge distributions in the LUMO levels of COF-TZ-1 and COF-TZ-2. The conversion of imine linkages into thiazole linkages inserts an electron acceptor into the COFs. Also, the theoretical E_g of COF-TZ-1 and COF-TZ-2 were 1.96 and 2.14 eV, respectively, which agrees well with the trend of the experimental results. The different orientations of linkages make great contributions on the band structures of the COFs.

Selective oxidation of organic sulfides is a vital oxidation reaction [50–52]. To explore the divergent photocatalysis, the four COFs, COF-TZ-1, COF-IM-1, COF-TZ-2, and COF-IM-2 were employed for
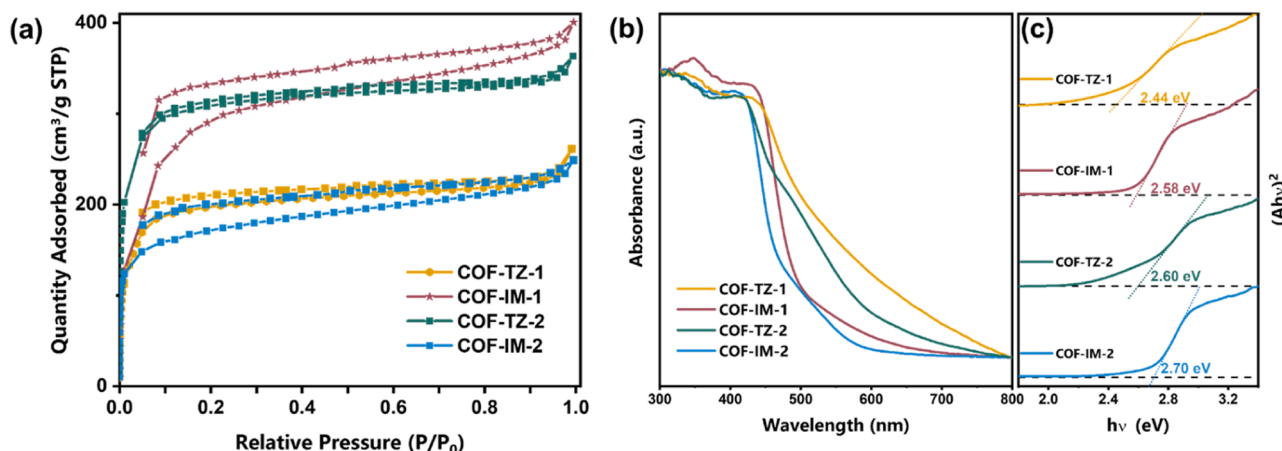

Fig. 5. The N_2 sorption isotherms (a), the UV–visible DRS (b), and corresponding Tauc plots (c) of COF-TZ-1, COF-IM-1, COF-TZ-2, and COF-IM-2.
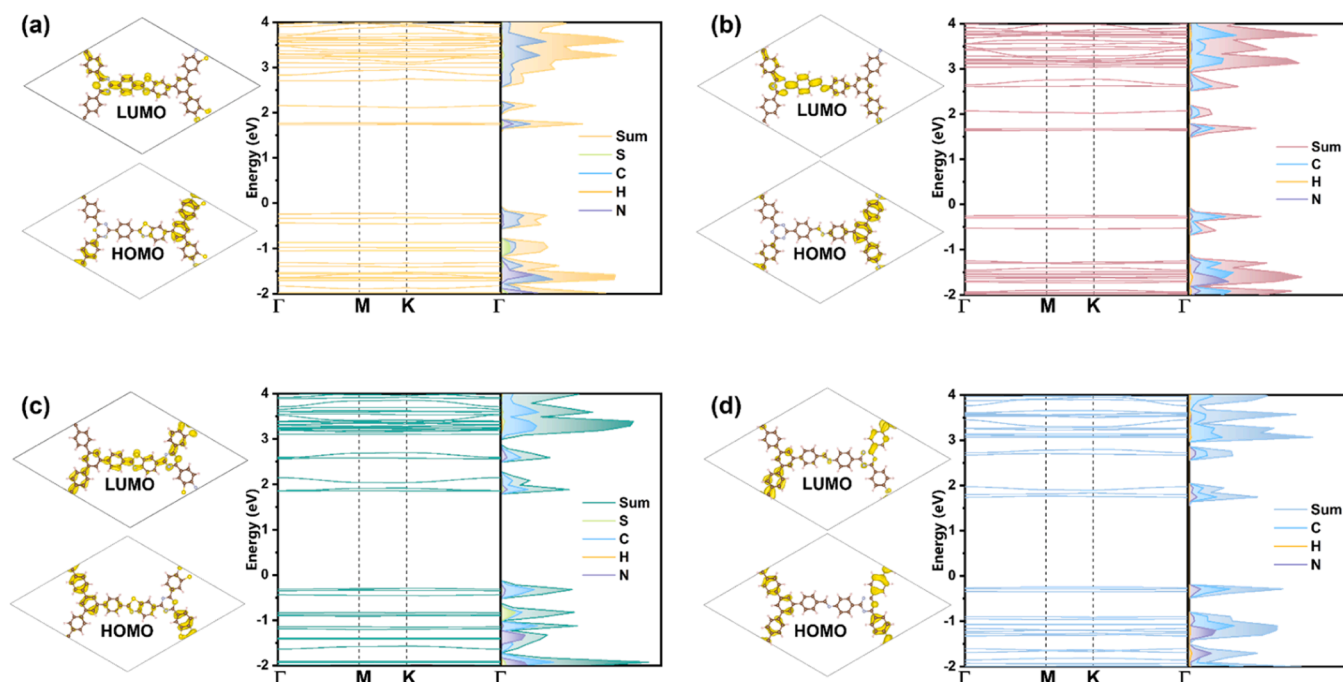
Fig. 6. The charge density distribution of LUMO and HOMO, band structure, and DOS of COF-TZ-1 (a), COF-IM-1 (b), COF-TZ-2 (c), and COF-IM-2 (d).

selective oxidation of organic sulfides. After the conversion of linkages, COF-TZ-1 and COF-TZ-2 displayed superior photocatalytic activity on the selective oxidation of sulfides to COF-IM-1 and COF-IM-2. Thereinto, COF-TZ-2 had the best photocatalytic activity. The reaction thoroughly completed within 15 min (Fig. 7a). Meanwhile, whether replacing the *para*-substituent of H atom with –CH$_3$ or –Cl, the conversions for photocatalytic selective oxidation of phenyl methyl sulfides over COF-TZ-1 and COF-TZ-2 far exceeded that over COF-IM-1 and COF-IM-2, respectively. Distinctly, the photocatalytic activity of COF-TZ-2 was superior to that of COF-TZ-1. Conclusively, the different orientation of the thiazole linkage impacts the photocatalytic activity of 2D COFs (Fig. 7b).

3.2. The divergent photocatalysis over the thiazole-linked isomeric COFs

Furthermore, the underpinning for divergent photocatalysis over COF-TZ-1 and COF-TZ-2 was investigated through theoretical and experimental results. The electrostatic potential (ESP) maps of COF-TZ-1 and COF-TZ-2 were generated based on the optimized molecular fragments (Fig. 8). The negative potential mainly converged on N of

thiazole, while the positive potential distributed in benzene. Due to the C_s symmetry of benzothiazole as an electron-withdrawing group in COFs, altering the orientation of the thiazole linkages made a difference in the dipole moment, afforded 1.63 Debye in COF-TZ-1 and 3.02 Debye in COF-TZ-2. In essence, bonding benzothiazole into benzene lowers the electron-donating capacity of benzene. However, the incorporation of triazine and benzothiazole formed a stronger electron-withdrawing fragment. Triphenylbenzene acted as the electron donor, corresponding well with a larger dipole moment in COF-TZ-2. Notably, a larger dipole moment contributes to aggravated polarization of the electric field, resulting in the promotion of charge separation and in-plane electron transfer [53–56].

The photoluminescence (PL) spectra, as well as the time-resolved PL spectra, were collected to evaluate the recombination dynamics of photoinduced charge carriers (Fig. 9a and b). There was a stronger PL intensity for COF-TZ-2 than that for COF-TZ-1. Moreover, the photoinduced carriers' lifetimes of COF-TZ-2 and COF-TZ-1 were 0.54 and 0.48 ns, respectively. The longer carrier lifetime of COF-TZ-2 is attributed to a larger dipole moment.
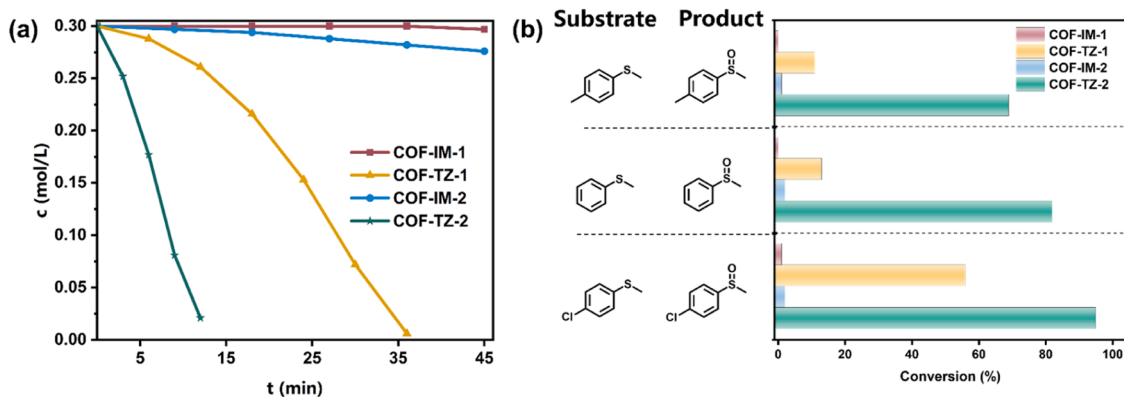

Fig. 7. (a) The kinetic curves of COF-IM-1, COF-TZ-1, COF-IM-2, and COF-TZ-2 for selective photocatalytic aerobic oxidation of phenyl methyl sulfide. (b) The difference in photocatalytic activity of COF-IM-1, COF-TZ-1, COF-IM-2, and COF-TZ-2 for selective aerobic oxidation of phenyl methyl sulfides. Reaction conditions: phenyl methyl sulfide (0.3 mmol), photocatalyst (4 mg), blue LED irradiation (460 ± 10 nm), O$_2$ (0.1 MPa), CH$_3$OH (1 mL). (b) 11 min.
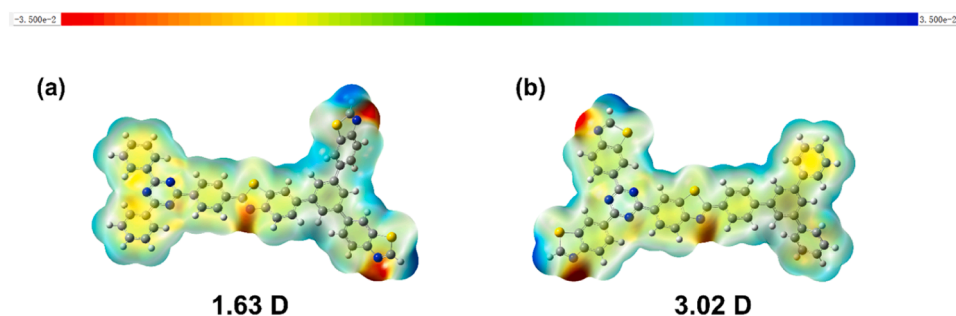
Fig. 8. The ESP mapping (red: negative potential; blue: positive potential) and dipole moments of COF-TZ-1 (a) and COF-TZ-2 (b).
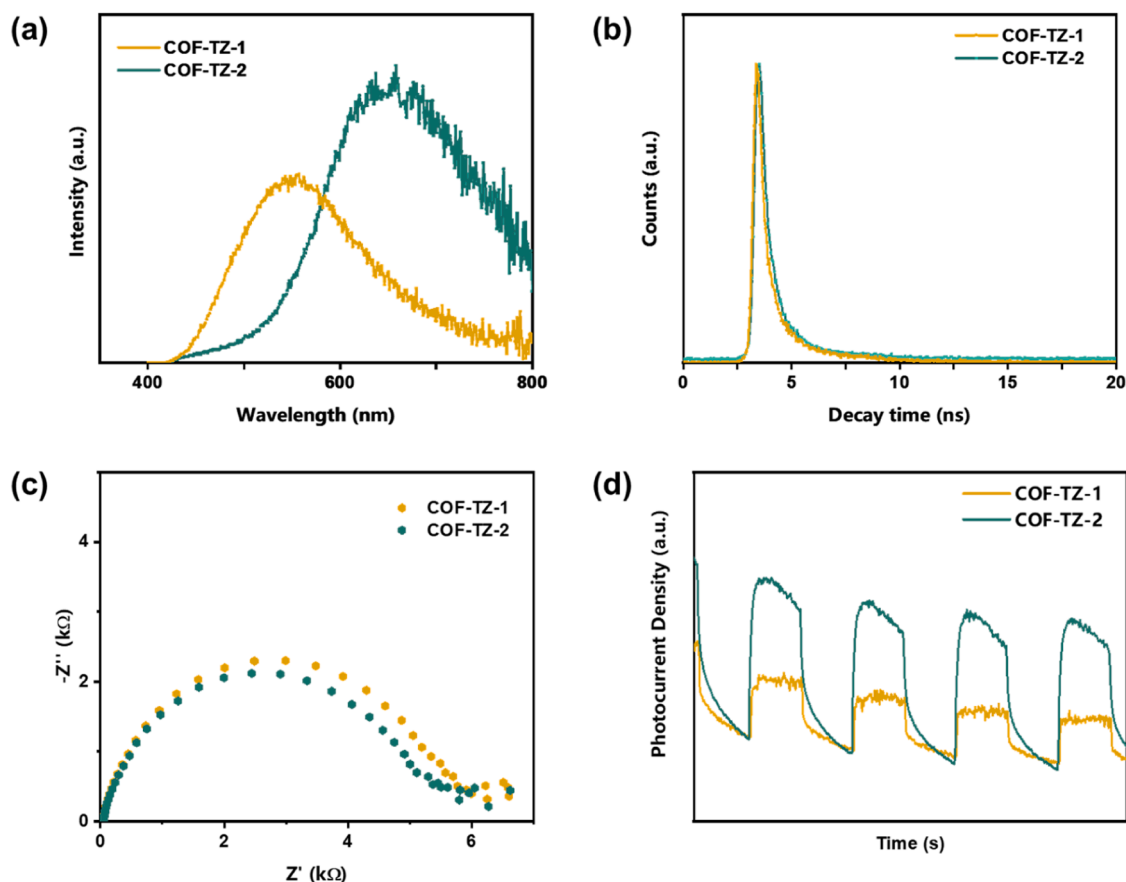

Fig. 9. The PL spectra (a), the time-resolved PL spectra (b), the EIS plots (c), and the transient photocurrent densities (d) of COF-TZ-1 and COF-TZ-2.

The photoelectrochemical properties of COF-TZ-1 and COF-TZ-2 were evaluated through transient photocurrents and electrochemical impedance spectroscopy (EIS). The radius of Nyquist arc of COF-TZ-1 was longer than that of COF-TZ-2 (Fig. 9c). Thus, COF-TZ-2 had less resistance and faster mobility in electron transfer than COF-TZ-1. Meanwhile, in contrast to the COF-TZ-1, COF-TZ-2 evidently showed higher photocurrent density during light on/off cycles (Fig. 9d), indicative of superior charge separation and transfer in COF-TZ-2 to that in COF-TZ-1. This trend also agrees well with a larger dipole moment of COF-TZ-2 than that of COF-TZ-1. Notably, transient photocurrents and EIS plots of COF-IM-1 and COF-IM-2 are also presented in Figure S7. Therefore, the conversion of imine linkages into thiazole linkages promotes the electron transfer over COFs. Both transient photocurrent densities and EIS plots attested that COF-TZ-2 owns superior optoelectronic properties caused by the different orientations of linkages. These have tremendous impact on COF-TZ-1 and COF-TZ-2 as visible light photocatalysts for the conversions of phenyl methyl sulfides.

3.3. Investigations on photocatalytic oxidation of sulfides over COF-TZ-2

Photocatalytic oxidation of organic sulfides is an energy-efficient and green approach for the production of highly value-added organic sulfoxides [57–59]. Thus, the oxidation of sulfides into targeted sulfoxides is highly preferred under ambient conditions. As described in Table S2, compared with that over COF-TZ-1 and COF-TZ-2, there were inferior conversions of phenyl methyl sulfide over COF-IM-1 and COF-IM-2 (Table S2, entries 1–4). Besides, the conversion over COF-TZ-2 for the photocatalytic oxidation of phenyl methyl sulfide was 5 times that of COF-TZ-1 with an excellent selectivity, emphasizing the importance of the different orientations of the thiazole linkage (Table S2, entries 1 and 3). Meanwhile, whether with the building blocks of 1,3,5-tris(4-amino-phenyl)triazine, 1,3,5-tris(4-formylphenyl)benzene, or S_8 as the photocatalyst, there were no conversions of phenyl methyl sulfide to phenyl methyl sulfoxide (Table S2, entries 5–9). Notably, there were also no conversions of phenyl methyl sulfide over the physical mixture of S_8 and

COF-IM-1 or COF-IM-2 (Table S2, entries 10 and 11). Without COF-TZ-2 or blue LED irradiation, there was also scarce conversion of phenyl methyl sulfide, indicating that COF-TZ-2 and light source are pre-requisites for photocatalytic oxidation of phenyl methyl sulfide (Table S2, entries 12 and 13). Notably, TEMPO (2,2,6,6-tetramethylpi-peridine-*N*-oxyl) has been widely exploited for cooperative photo-catalysis over semiconductors [60]. However, for selective oxidation of phenyl methyl sulfide over COF-TZ-2, adding 1% TEMPO inhibited the conversion of phenyl methyl sulfide from 83% to 13% under the same conditions. Besides, the PXRD pattern further verified the stability of COF-TZ-2 after photocatalytic oxidation of phenyl methyl sulfide (Figure S8). Notably, COF-TZ-2, after the reaction, retained the relative intensity of the characteristic peaks, suggesting that COF-TZ-2 is stable enough for reusable photocatalytic reactions. Utilization of visible light for photocatalytic oxidation of phenyl methyl sulfide over COF-TZ-2 was considered under the irradiation of different peak wavelengths of LEDs (Fig. 10a). Under green LED irradiation, COF-TZ-2 showed very mod-erate conversion of phenyl methyl sulfide with O_2. However, under blue and violet LED irradiation, the conversions of phenyl methyl sulfide with O_2 were saliently promoted, coinciding well with the UV–visible DRS (Fig. 5b). Meanwhile, the light-emission spectrum of the blue LED was measured (Figure S9), which overlaps thoroughly by the absorption of COF-TZ-2. Considering practicality, blue LEDs were selected for the ensuing reaction.

The recycling test was conducted to monitor the stability of COF-TZ-2 for photocatalytic selective oxidation of phenyl methyl sulfide (Fig. 10b). After four cycles, the reused COF-TZ-2 as the photocatalyst still maintained outstanding efficiency in the conversions of phenyl methyl sulfide. Besides, COF-TZ-2 maintained excellent selectivity in four cycles. COF-TZ-2 has superior recycling durability. This is highly favored for the practical utilization of COF-TZ-2 in photocatalysis. Moreover, the comparison of COF-TZ-2 with other photocatalysts re-ported in the literature is tabulated in Table S3. Evidently, COF-TZ-2 is superior to the other porous organic materials in the photocatalytic oxidation of organic sulfide.

The adsorption of O_2 over COF-TZ-2 was evaluated through DFT calculations of the adsorption energy (E_{ads}) of O_2 on different sites of COF-TZ-2 (Fig. 11a). Convincingly, the adsorption of O_2 is favored at the thiazole linkage of COF-TZ-2, corresponding to the more negative E_{ads}. Photocatalytic oxidation usually are initiated by ROS (reactive oxygen species) from O_2 [61–64]. In order to ascertain the ROS in the photo-catalytic selective oxidation of sulfide, quenching tests were executed meticulously through the addition of scavengers and maintainers (Fig. 11b). The presence of $AgNO_3$ as an e^- (electron) scavenger, or KI as an h^+ (hole) scavenger, inhibited the reaction remarkably. Thus,

photoinduced h^+ and e^- are the prerequisites for this reaction. Filling N_2 instead of O_2 into the atmosphere, the photocatalytic oxidation of phenyl methyl sulfide was restrained utterly, emphasizing the signifi-cance of O_2. When $O_2^{\bullet-}$ was captured by *p*-benzoquinone (*p*-BQ), the conversion of phenyl methyl sulfide was lowered, evidencing that $O_2^{\bullet-}$ makes a critical contribution as ROS. Replacing CH_3OH with CD_3OD to prolong the lifetime of singlet oxygen ($^1O_2$), no notable increase in the conversion of phenyl methyl sulfide was observed compared to the standard reaction, implying that there is no notable contribution of $^1O_2$ to the conversion of phenyl methyl sulfide.

Electron paramagnetic resonance (EPR) spectroscopy was applied to further confirm the plausible mechanism of photocatalytic selective oxidation of sulfide over COF-TZ-2 (Fig. 12). The signals of e^- appeared after 2 min of blue light irradiation and were further amplified with time, manifesting that COF-TZ-2 is able to produce e^- under blue light irradiation (Fig. 12a). However, exposing to an O_2 atmosphere, the signals of e^- disappeared completely, which was assigned to the transfer of e^- from LUMO of COF-TZ-2 to O_2. Then O_2 was reduced to $O_2^{\bullet-}$, and the signals of DMPO (5,5-dimethyl-1-pyrroline-*N*-oxide) trapped $O_2^{\bullet-}$ were described in Fig. 12b. With increasing time of blue light irradia-tion, the production of $O_2^{\bullet-}$ persistently occurred, suggesting that $O_2^{\bullet-}$ as ROS plays a critical role in the photocatalytic selective oxidation of phenyl methyl sulfide.

In brief, a plausible mechanism is put forward based on the experi-mental and theoretical results (Fig. 13). COF-TZ-2 as the photocatalyst is excited under blue LED irradiation, generating e^- and h^+. The former is consumed by O_2, producing $O_2^{\bullet-}$. Besides, phenyl methyl sulfide is oxidized by h^+ into the corresponding S-centred radical cation. Mean-while, produced radical cation further reacts with $O_2^{\bullet-}$, affording a vital immediate phenyl methyl persulfoxide. Consequently, the targeted product of phenyl methyl sulfoxide is afforded through the incorpora-tion of electrons and protons from CH_3OH with phenyl methyl persulf-oxide, acompanied with the production of H_2O.

To evaluate the universality of COF-TZ-2 in photocatalytic selective aerobic oxidation of sulfide, different phenyl methyl sulfides with various substituents were investigated as substrates (Table 1). Overall, the introduction of different halogen substituents on the phenyl ring of phenyl methyl sulfide needed more reaction time for a comparable conversion in the oxidation of sulfides with excellent selectivities (Table 1, entries 1–7). Following the electronegativity of *para*-substituted halogen substituents, the inhibiting effect receded gradually (Table 1, entries 1–3, 6, and 7). Installing −Cl as the substituent on the phenyl ring, the suppression effect abided by *ortho*- > *meta*- > *para*-substituted sequences (Table 1, entries 3–5). In contrast, −CH_3 as the *para*-substituent on the phenyl ring needed less reaction time for a
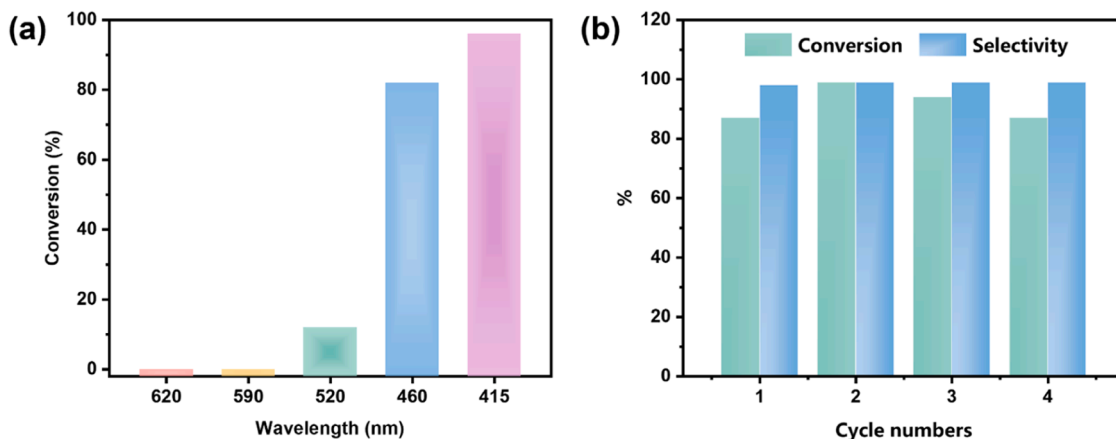

Fig. 10. (a) The influence of LEDs of various peak wavelengths on the selective oxidation of phenyl methyl sulfide over COF-TZ-2. (b) The recycling of COF-TZ-2 for the photocatalytic selective aerobic oxidation of phenyl methyl sulfide. Reaction conditions: phenyl methyl sulfide (0.3 mmol), COF-TZ-2 (4 mg), O_2 (0.1 MPa), CH_3OH (1 mL), 11 min. (a) LED irradiation (3 W × 4); (b) blue LED irradiation (460 ± 10 nm).
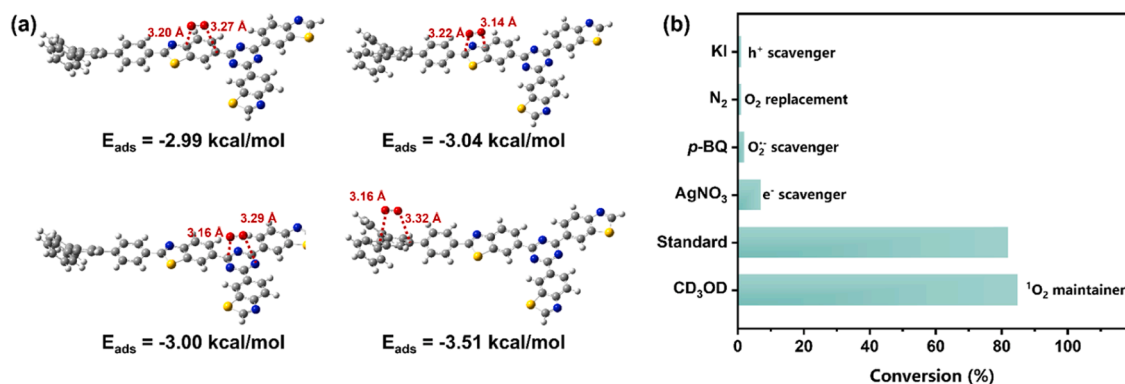
Fig. 11. (a) The four adsorption modes of O_2 on COF-TZ-2 and the corresponding adsorption energies. (b) The control experiments on the photocatalytic activity over COT-TZ-2 for selective aerobic oxidation of phenyl methyl sulfide. Standard conditions: phenyl methyl sulfide (0.3 mmol), COF-TZ-2 (4 mg), blue LED irradiation (460 ± 10 nm), O_2 (0.1 MPa), CH_3OH (1 mL), 11 min.
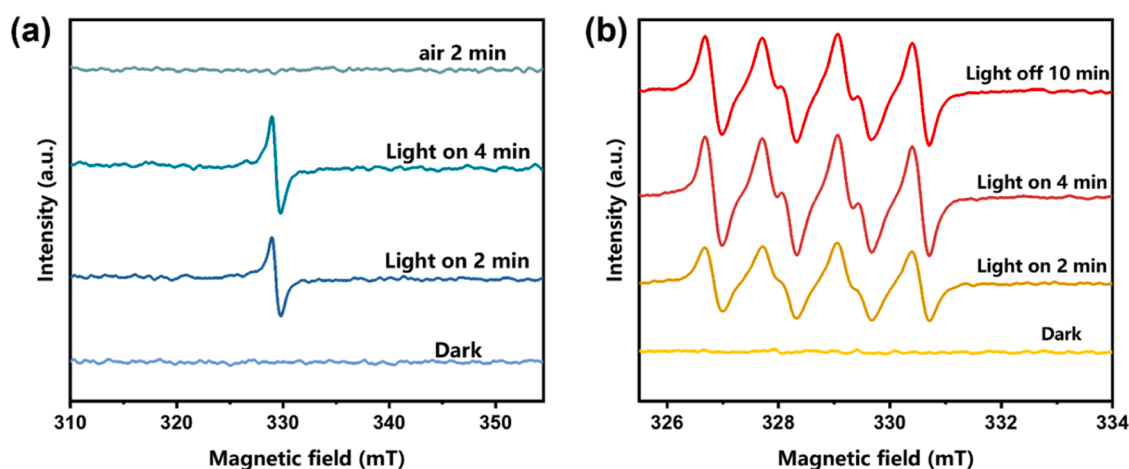

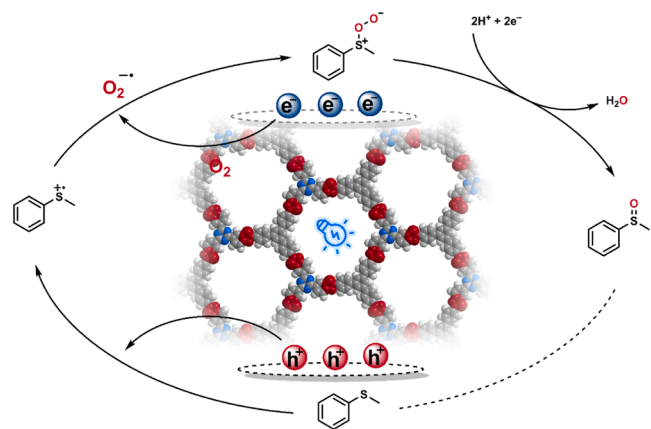**Fig. 12.** The EPR spectra of e^- (a) and DMPO trapped $O_2^{\bullet-}$ (b).

Fig. 13. A plausible mechanism for photocatalytic selective aerobic oxidation of sulfide over COF-TZ-2 under blue LED irradiation.

comparable conversion in the oxidation of phenyl methyl sulfide (Table 1, entry 8). Notably, the position of $-OCH_3$ made an evident influence on this reaction and the photocatalytic oxidation of substituted phenyl methyl sulfides with *para-*, *ortho-*, and *meta*-substitutions needed similar reaction time for comparable conversions of > 90% (Table 1, entries 9–11). Besides, $-NO_2$ *para*-substituted phenyl methyl sulfide was oxidized into the corresponding sulfoxide although needed much more

time (Table 1, entry 12).

Furthermore, other typical organic sulfides were tested as the substrates for selective aerobic oxidation over COF-TZ-2 under blue LED irradiation (Table 2). There were also successful conversions of aliphatic sulfides, including linear or cyclic ones (Table 2, entries 1 and 2). The oxidation of phenyl ethyl sulfide was completed within 20 min (Table 2, entry 3). When the phenyl ring was replaced with a naphthalene ring, or replacing the methyl group with a phenyl ring, the comparable conversions of sulfide needed much longer reaction time but with very satisfactory selectivities (Table 2, entries 4 and 5).
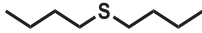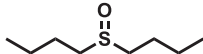
4. Conclusions
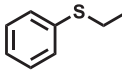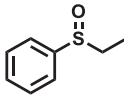
To summarize, two thiazole-linked isomeric 2D COFs, COF-TZ-1 and COF-TZ-2, with different orientations of thiazole linkage, have been successfully constructed from two imine-linked isomeric 2D COFs, COF-IM-1 and COF-IM-2, respectively. Intriguingly, the four COFs possessed well-defined crystal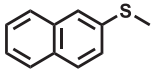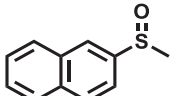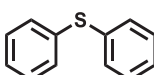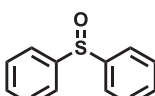linity and porosity. The structure–activity relationship between isomeric linkages and COF photocatalysis was meticulously explored through experimental and theoretical efforts. Significantly, the transformation of the imine-linked COFs into the thiazole-linked COFs played a vital role in determining the photocatalytic activity in selective oxidation of sulfides under blue LED irradiation. Besides, COF-TZ-2 had a larger dipole moment than COF-TZ-1, resulting in superior charge separation and in-plane electron transfer. Hence, COF-TZ-2 exhibited the best photocatalytic activity for the selective oxidation of organic sulfides with O_2 among the two imine-linked

Table 1

Selective aerobic oxidation of phenyl methyl sulfides to phenyl methyl sulfoxides over COF-TZ-2 under blue LED irradiation[a].

Entry	Substrate	Product	t (min)	Conv. (%)	Sel. (%)
1			13	93	99
2			13	90	99
3			15	91	97
4			35	90	97
5			25	95	97
6			15	93	93
7			25	91	95
8			11	95	97
9			15	90	96
10			18	92	94
11			18	96	96
12			175	92	87

[a] Reaction conditions: COF-TZ-2 (4 mg), organic sulfide (0.3 mmol), blue LED irradiation (460 $\pm$ 10 nm), O$_2$ (0.1 MPa), CH$_3$OH (1 mL).

Table 2

Selective aerobic oxidation of the other typical organic sulfides to sulfoxides over COF-TZ-2 under blue LED irradiation[a].

Entry	Substrate	Product	t (min)	Conv. (%)	Sel. (%)
1			9	90	88
2			10	90	99
3			16	93	80
4			90	95	90
5			96	>99	97

[a] Reaction conditions: COF-TZ-2 (4 mg), organic sulfide (0.3 mmol), blue LED irradiation (460 $\pm$ 10 nm), O_2 (0.1 MPa), CH_3OH (1 mL).

COFs of COF-IM-1 and COF-IM-2 and the two thiazole-linked COFs of COF-TZ-1 and COF-TZ-2. Notably, mechanistic studies revealed that $O_2^{\bullet-}$ plays a critical role as ROS in this reaction. In the end, a plausible mechanism of the reaction was put forward through the incorporation of experimental and theoretical results. This work reveals that the different orientation of the linkage make significant contributions to the divergent photocatalytic activity over COFs.

CRediT authorship contribution statement

Yuexin Wang: Writing – original draft, Investigation, Formal analysis. **Fulin Zhang:** Investigation, Formal analysis. **Fengwei Huang:** Investigation, Formal analysis. **Xiaoyun Dong:** Investigation, Formal analysis, Conceptualization. **Bing Zeng:** Investigation, Formal analysis. **Xiang-Kui Gu:** Investigation, Formal analysis. **Xianjun Lang:** Writing – review & editing, Supervision, Funding acquisition, Conceptualization.

Declaration of Competing Interest

The authors declare that they have no known competing financial interests or personal relationships that could have appeared to influence the work reported in this paper.

Data availability

Data will be made available on request.

Acknowledgments

Appendix A. Supporting information

Supplementary data associated with this article can be found in the online version at doi:10.1016/j.apcatb.2024.124103.

References

[1] Y.N. Gong, X.Y. Guan, H.L. Jiang, Covalent organic frameworks for photocatalysis: Synthesis, structural features, fundamentals and performance, Coord. Chem. Rev. 475 (2023) 214889, https://doi.org/10.1016/j.ccr.2022.214889.

[2] Q.Q. Tang, Y.Y. Gu, J. Ning, Y.K. Yan, L. Shi, M.S. Zhou, H.T. Wei, X.H. Ren, X. H. Li, J.X. Wang, C. Tang, L. Hao, J.H. Ye, Boosting photocatalysis of hydrazone-linked covalent organic frameworks through introducing electron-rich conjugated aldehyde, Chem. Eng. J. 470 (2023) 144106, https://doi.org/10.1016/j.cej.2023.144106.

[3] C.J. Wu, M.Z. Shao, Y. Geng, Y.B. Dong, Photochemical synthesis of covalent organic frameworks, ChemCatChem 15 (2023) e202300244, https://doi.org/10.1002/cctc.202300244.

[4] M.J. Hao, Z.S. Chen, X.L. Liu, X.H. Liu, J.Y. Zhang, H. Yang, G.I.N. Waterhouse, X. K. Wang, S.Q. Ma, Converging cooperative functions into the nanospace of covalent organic frameworks for efficient uranium extraction from seawater, CCS Chem. 4 (2022) 2294–2307, https://doi.org/10.31635/ccschem.022.202201897.

[5] X.Y. Guan, Y.Y. Qian, X.Y. Zhang, H.L. Jiang, Enaminone-linked covalent organic frameworks for boosting photocatalytic hydrogen production, Angew. Chem. Int. Ed. 62 (2023) e202306135, https://doi.org/10.1002/anie.202306135.

[6] Z.P. Xie, X.B. Yang, P. Zhang, X.T. Ke, X. Yuan, L.P. Zhai, W.B. Wang, N. Qin, C. X. Cui, L.B. Qu, X. Chen, Vinylene-linked covalent organic frameworks with manipulated electronic structures for efficient solar-driven photocatalytic hydrogen production, Chin. J. Catal. 47 (2023) 171–180, https://doi.org/10.1016/s1872-2067(23)64397-9.

[7] H. Wang, C. Qian, J. Liu, Y.F. Zeng, D.D. Wang, W.Q. Zhou, L. Gu, H.W. Wu, G. F. Liu, Y.L. Zhao, Integrating suitable linkage of covalent organic frameworks into covalently bridged inorganic/organic hybrids toward efficient photocatalysis, J. Am. Chem. Soc. 142 (2020) 4862–4871, https://doi.org/10.1021/jacs.0c00054.

[8] F.D. Wang, L.J. Yang, X.X. Wang, Y. Rong, L.B. Yang, C.X. Zhang, F.Y. Yan, Q. L. Wang, Pyrazine-functionalized donor–acceptor covalent organic frameworks for enhanced photocatalytic H_2 evolution with high proton transport, Small 19 (2023) 2207421, https://doi.org/10.1002/smll.202207421.

[9] F.L. Zhang, X. Li, X.Y. Dong, H.M. Hao, X.J. Lang, Thiazolo[5,4-d]thiazole-based covalent organic framework microspheres for blue light photocatalytic selective oxidation of amines with O_2, Chin. J. Catal. 43 (2022) 2395–2404, https://doi.org/10.1016/S1872-2067(22)64127-5.

[10] Y. Kondo, K. Hino, Y. Kuwahara, K. Mori, H. Yamashita, Photosynthesis of hydrogen peroxide from dioxygen and water using aluminium-based metal–organic framework assembled with porphyrin- and pyrene-based linkers, J. Mater. Chem. A 11 (2023) 9530–9537, https://doi.org/10.1039/d3ta01051a.

[11] C.J. Wu, X.Y. Li, T.R. Li, M.Z. Shao, L.J. Niu, X.F. Lu, J.L. Kan, Y. Geng, Y.B. Dong, Natural sunlight photocatalytic synthesis of benzoxazole-bridged covalent organic framework for photocatalysis, J. Am. Chem. Soc. 144 (2022) 18750–18755, https://doi.org/10.1021/jacs.2c07893.

[12] Z.F. Wang, Y.S. Zhang, T. Wang, E. Lin, Y. Chen, P. Cheng, Z.J. Zhang, Modulating the interlayer stacking of covalent organic frameworks for efficient acetylene separation, Small 19 (2023) 2303684, https://doi.org/10.1002/smll.202303684.

[13] S. Wang, Y.H. Yang, H.R. Zhang, Z.Y. Zhang, C. Zhang, X.D. Huang, D.C. Kozawa, P.W. Liu, B.G. Li, W.J. Wang, Toward covalent organic framework metastructures, J. Am. Chem. Soc. 143 (2021) 5003–5010, https://doi.org/10.1021/jacs.0c13090.

[14] J. Zhang, C. Cheng, L.J. Guan, H.L. Jiang, S.B. Jin, Rapid synthesis of covalent organic frameworks with a controlled morphology: An emulsion polymerization approach via the phase transfer catalysis mechanism, J. Am. Chem. Soc. 145 (2023) 21974–21982, https://doi.org/10.1021/jacs.3c06764.

[15] T. Wang, M.J. Li, Y.J. Chen, X.P. Che, F.Z. Bi, Y. Yang, R.Q. Yang, C.X. Li, Regioisomeric benzotriazole-based covalent organic frameworks for high photocatalytic activity, ACS Catal. 13 (2023) 15439–15447, https://doi.org/10.1021/acscatal.3c04145.

[16] W.J. Weng, J. Guo, The effect of enantioselective chiral covalent organic frameworks and cysteine sacrificial donors on photocatalytic hydrogen evolution, Nat. Commun. 13 (2022) 5768, https://doi.org/10.1038/s41467-022-33501-8.

[17] P. Albacete, J.I. Martínez, X. Li, A. López-Moreno, S. Mena-Hernando, A.E. Platero-Prats, C. Montoro, K.P. Loh, E.M. Pérez, F. Zamora, Layer-stacking-driven fluorescence in a two-dimensional imine-linked covalent organic framework, J. Am. Chem. Soc. 140 (2018) 12922–12929, https://doi.org/10.1021/jacs.8b07450.

[18] C.F. Lu, Y.P. Mo, Y. Hong, T. Chen, Z.Y. Yang, L.J. Wan, D. Wang, On-surface growth of single-layered homochiral 2D covalent organic frameworks by steric hindrance strategy, J. Am. Chem. Soc. 142 (2020) 14350–14356, https://doi.org/10.1021/jacs.0c06468.

[19] S.X. Yang, T.C. Li, Y. Cheng, W.W. Fan, L.J. Wang, Y.X. Liu, L.C. Bian, C.H. Zhou, L.Y. Zheng, Q.E. Cao, Covalent organic framework isomers for photoenhanced gold recovery from e-waste with high efficiency and selectivity, ACS Sustainable Chem. Eng. 10 (2022) 9719–9731, https://doi.org/10.1021/acssuschemeng.2c00285.

[20] Y.Z. Liu, J.W. Li, J. Lv, Z.T. Wang, J.Q. Suo, J.X. Ren, J.C. Liu, D. Liu, Y.J. Wang, V. Valtchev, S.L. Li, D.L. Zhang, Q.R. Fang, Topological isomerism in three-dimensional covalent organic frameworks, J. Am. Chem. Soc. 145 (2023) 9679–9685, https://doi.org/10.1021/jacs.3c01070.

[21] R.R. Liang, F.Z. Cui, R.H. A, Q.Y. Qi, X. Zhao, A study on constitutional isomerism in covalent organic frameworks: Controllable synthesis, transformation, and distinct difference in properties, CCS Chem. 2 (2020) 139–145, https://doi.org/10.31635/ccschem.020.201900094.

[22] T.Q. Ma, J. Li, J. Niu, L. Zhang, A.S. Etman, C. Lin, D.E. Shi, P.H. Chen, L.H. Li, X. Du, J.L. Sun, W. Wang, Observation of interpenetration isomerism in covalent organic frameworks, J. Am. Chem. Soc. 140 (2018) 6763–6766, https://doi.org/10.1021/jacs.8b03169.

[23] B. Gui, J.J. Xin, Y.P. Cheng, Y.F. Zhang, G.Q. Lin, P.H. Chen, J.X. Ma, X. Zhou, J.L. Sun, C. Wang, Crystallization of dimensional isomers in covalent organic frameworks, J. Am. Chem. Soc. 145 (2023) 11276–11281, https://doi.org/10.1021/jacs.3c01729.

[24] W.B. Chen, P. Chen, D. Chen, Y. Liu, G. Zhang, L. Wang, L. Chen, Triangular topological 2D covalent organic frameworks constructed via symmetric or asymmetric "two-in-one" type monomers, Adv. Sci. 9 (2022) 2105517, https://doi.org/10.1002/advs.202105517.

[25] J.X. Fu, Y. Liu, L.H. Chen, W.K. Han, X. Liu, J.X. Shao, X.D. Yan, Z.G. Gu, Positional isomers of covalent organic frameworks for indoor humidity regulation, Small 19 (2023) 2303897, https://doi.org/10.1002/smll.202303897.

[26] S.X. Li, R. Ma, S.Q. Xu, T.Y. Zheng, G.G. Fu, Y.L. Wu, Z.Q. Liao, Y.B. Kuang, Y. Hou, D.S. Wang, P.S. Petkov, K. Simeonova, X.L. Feng, L.Z. Wu, X.B. Li, T. Zhang, Direct construction of isomeric benzobisoxazole–vinylene-linked covalent organic frameworks with distinct photocatalytic properties, J. Am. Chem. Soc. 144 (2022) 13953–13960, https://doi.org/10.1021/jacs.2c06042.

[27] F. Yang, H.Y. Qu, Y. Guo, J.L. Kan, Y.B. Dong, Boosting the photocatalytic performance *via* isomeric configuration design in covalent organic frameworks, Chem. Commun. 58 (2022) 13210–13213, https://doi.org/10.1039/d2cc04935j.

[28] J. Yang, S. Ghosh, J. Roeser, A. Acharjya, C. Penschke, Y. Tsutsui, J. Rabeah, T.Y. Wang, S.Y.D. Tameu, M.Y. Ye, J. Grüneberg, S. Li, C.X. Li, R. Schomäcker, R. Van de Krol, S. Seki, P. Saalfrank, A. Thomas, Constitutional isomerism of the linkages in donor–acceptor covalent organic frameworks and its impact on photocatalysis, Nat. Commun. 13 (2022) 6317, https://doi.org/10.1038/s41467-022-34092-0.

[29] W.B. Dong, Z.Y. Qin, K.X. Wang, Y.Y. Xiao, X.Y. Liu, S.J. Ren, L.Y. Li, Isomeric oligo (phenylenevinylene)-based covalent organic frameworks with different orientation of imine bonds and distinct photocatalytic activities, Angew. Chem. Int. Ed. 62 (2022) e202216073, https://doi.org/10.1002/anie.202216073.

[30] M.C. Zhang, X. Wu, Y.B. Xie, X.L. Hao, Q.H. Wang, Y.Q. Zhao, J.C. Wu, X.B. Pan, Effect of COF linkage isomerism on photocatalytic hydrogen evolution performance, Mater. Chem. Front. 7 (2023) 5399–5405, https://doi.org/10.1039/d3qm00807j.

[31] X.H. Liu, Y.P. Mo, J.Y. Yue, Q.N. Zheng, H.J. Yan, D. Wang, L.J. Wan, Isomeric routes to Schiff-base single-layered covalent organic frameworks, Small 10 (2014) 4934–4939, https://doi.org/10.1002/smll.201400899.

[32] S.Q. Xu, R.R. Liang, T.G. Zhan, Q.Y. Qi, X. Zhao, Construction of 2D covalent organic frameworks by taking advantage of the variable orientation of imine bonds, Chem. Commun. 53 (2017) 2431–2434, https://doi.org/10.1039/c6cc09906h.

[33] S. Ghosh, Y. Tsutsui, K. Suzuki, H. Kaji, K. Honjo, T. Uemura, S. Seki, Impact of the position of the imine linker on the optoelectronic performance of π-conjugated organic frameworks, Mol. Syst. Des. Eng. 4 (2019) 325–331, https://doi.org/10.1039/c8me00079d.

[34] V. Singh, J. Kim, B. Kang, J. Moon, S. Kim, W.Y. Kim, H.R. Byon, Thiazole-linked covalent organic framework promoting fast two-electron transfer for lithium-organic batteries, Adv. Energy Mater. 11 (2021) 2003735, https://doi.org/10.1002/aenm.202003735.

[35] Y.H. Kim, N. Kim, J.M. Seo, J.P. Jeon, H.J. Noh, D.H. Kweon, J. Ryu, J.B. Baek, Benzothiazole-based covalent organic frameworks with different symmetrical

[36] H. Wan, S. Wang, H. Chen, L. Chen, Y. Song, L. Wang, Fluorescent benzothiazole-based covalent-organic frameworks with intramolecular dual "lock" for ratiometric detection of fenthion, Mater. Today Chem. 26 (2022) 101178, https://doi.org/10.1016/j.mtchem.2022.101178.

[37] A. López-Magano, S. Daliran, A.R. Oveisi, R. Mas-Ballesté, A. Dhakshinamoorthy, J. Alemán, H. Garcia, R. Luque, Recent advances in the use of covalent organic frameworks as heterogenous photocatalysts in organic synthesis, Adv. Mater. 35 (2023) 2209475, https://doi.org/10.1002/adma.202209475.

[38] Y.F. Zhi, Z.P. Li, X. Feng, H. Xia, Y.M. Zhang, Z. Shi, Y. Mu, X.M. Liu, Covalent organic frameworks as metal-free heterogeneous photocatalysts for organic transformations, J. Mater. Chem. A 5 (2017) 22933–22938, https://doi.org/10.1039/c7ta07691f.

[39] H. Chen, H.S. Jena, X. Feng, K. Leus, P. Van der Voort, Engineering covalent organic frameworks as heterogeneous photocatalysts for organic transformations, Angew. Chem. Int. Ed. 61 (2022) e202204938, https://doi.org/10.1002/anie.202204938.

[40] Z.J. Gu, J.J. Wang, Z. Shan, M.M. Wu, T.T. Liu, L. Song, G.X. Wang, X.H. Ju, J. Su, G. Zhang, Modulating electronic structure of triazine-based covalent organic frameworks for photocatalytic organic transformations, J. Mater. Chem. A 10 (2022) 17624–17632, https://doi.org/10.1039/d2ta04541a.

[41] G.B. Wang, K.H. Xie, H.P. Xu, Y.J. Wang, F. Zhao, Y. Geng, Y.B. Dong, Covalent organic frameworks and their composites as multifunctional photocatalysts for efficient visible-light induced organic transformations, Coord. Chem. Rev. 472 (2022) 214774, https://doi.org/10.1016/j.ccr.2022.214774.

[42] Z.P. Li, Y.F. Zhi, P.P. Shao, H. Xia, G.S. Li, X. Feng, X. Chen, Z. Shi, X.M. Liu, Covalent organic framework as an efficient, metal-free, heterogeneous photocatalyst for organic transformations under visible light, Appl. Catal. B 245 (2019) 334–342, https://doi.org/10.1016/j.apcatb.2018.12.065.

[43] P. Costa, A. Vega-Peñaloza, L. Cognigni, M. Bonchio, Light-induced organic transformations by covalent organic frameworks as reticular platforms for selective photosynthesis, ACS Sustainable Chem. Eng. 9 (2021) 15694–15721, https://doi.org/10.1021/acssuschemeng.1c04787.

[44] Y.X. Wang, F.W. Huang, W.L. Sheng, X. Miao, X. Li, X.K. Gu, X.J. Lang, Blue light photocatalytic oxidation of sulfides to sulfoxides with oxygen over a thiazole-linked 2D covalent organic framework, Appl. Catal. B 338 (2023) 123070, https://doi.org/10.1016/j.apcatb.2023.123070.

[45] J. Yang, A. Acharjya, M.Y. Ye, J. Rabeah, S. Li, Z. Kochovski, S. Youk, J. Roeser, J. Gruneberg, C. Penschke, M. Schwarze, T.Y. Wang, Y. Lu, R. van de Krol, M. Oschatz, R. Schomacker, P. Saalfrank, A. Thomas, Protonated imine-linked covalent organic frameworks for photocatalytic hydrogen evolution, Angew. Chem. Int. Ed. 60 (2021) 19797–19803, https://doi.org/10.1002/anie.202104870.

[46] F. Haase, E. Troschke, G. Savasci, T. Banerjee, V. Duppel, S. Dörfler, M.M.J. Grundei, A.M. Burow, C. Ochsenfeld, S. Kaskel, B.V. Lotsch, Topochemical conversion of an imine-into a thiazole-linked covalent organic framework enabling real structure analysis, Nat. Commun. 9 (2018) 2600, https://doi.org/10.1038/s41467-018-04979-y.

[47] S. Ma, Z.P. Li, J. Jia, Z.W. Zhang, H. Xia, H. Li, X. Chen, Y.H. Xu, X.M. Liu, Amide-linked covalent organic frameworks as efficient heterogeneous photocatalysts in water, Chin. J. Catal. 42 (2021) 2010–2019, https://doi.org/10.1016/s1872-2067(21)63836-6.

[48] Y.J. Zou, S. Abednatanzi, P.G. Derakhshandeh, S. Mazzanti, C.M. Schusslbauer, D. Cruz, P. Van der Voort, J.W. Shi, M. Antonietti, D.M. Guldi, A. Savateev, Red edge effect and chromoselective photocatalysis with amorphous covalent triazine-based frameworks, Nat. Commun. 13 (2022) 2171, https://doi.org/10.1038/s41467-022-29781-9.

[49] J.Y. Guo, D.G. Ma, F.L. Sun, G.L. Zhuang, Q. Wang, A.M. Al-Enizi, A. Nafady, S.Q. Ma, Substituent engineering in g-C₃N₄/COF heterojunctions for rapid charge separation and high photo-redox activity, Sci. China Chem. 65 (2022) 1704–1709, https://doi.org/10.1007/s11426-022-1350-1.

[50] M.A. Hoque, J.B. Gerken, S.S. Stahl, Synthetic dioxygenase reactivity by pairing electrochemical oxygen reduction and water oxidation, Science 383 (2024) 173–178, https://doi.org/10.1126/science.adk5097.

[51] Y.K. Zhao, C.Y. Deng, D.J. Tang, L.Y. Ding, Y.C. Zhang, H. Sheng, H.W. Ji, W.J. Song, W.H. Ma, C.C. Chen, J.C. Zhao, α-Fe₂O₃ as a versatile and efficient oxygen atom transfer catalyst in combination with H₂O as the oxygen source, Nat. Catal. 4 (2021) 684–691, https://doi.org/10.1038/s41929-021-00659-1.

[52] S. Fukuzumi, T. Kishi, H. Kotani, Y.M. Lee, W. Nam, Highly efficient photocatalytic oxygenation reactions using water as an oxygen source, Nat. Chem. 3 (2011) 38–41, https://doi.org/10.1038/nchem.905.

[53] H.J. Ben, G.J. Yan, H.Y. Liu, C.C. Ling, Y. Fan, X.J. Zhang, Local spatial polarization induced efficient charge separation of squaraine-linked COF for enhanced photocatalytic performance, Adv. Funct. Mater. 32 (2022) 2104519, https://doi.org/10.1002/adfm.202104519.

[54] Z.S. Chen, J.Y. Wang, M.J. Hao, Y.H. Xie, X.L. Liu, H. Yang, G.I.N. Waterhouse, X.K. Wang, S.Q. Ma, Tuning excited state electronic structure and charge transport in covalent organic frameworks for enhanced photocatalytic performance, Nat. Commun. 14 (2023) 1106, https://doi.org/10.1038/s41467-023-36710-x.

[55] C.B. Wu, Z.Y. Teng, C. Yang, F.S. Chen, H.Bin Yang, L. Wang, H.X. Xu, B. Liu, G.F. Zheng, Q. Han, Polarization engineering of covalent triazine frameworks for highly efficient photosynthesis of hydrogen peroxide from molecular oxygen and water, Adv. Mater. 34 (2022) 2110266, https://doi.org/10.1002/adma.202110266.

[56] K. Wu, X.Y. Liu, M. Xie, P.W. Cheng, J. Zheng, W.G. Lu, D. Li, Rational design of D−π−A−π−D porous organic polymer with polarized π for photocatalytic aerobic

oxidation, Appl. Catal. B 334 (2023) 122847, https://doi.org/10.1016/j.apcatb.2023.122847.

[57] F.W. Huang, Y.X. Wang, X.Y. Dong, X.J. Lang, Merging benzotrithiophene covalent organic framework photocatalysis with TEMPO for selective oxidation of organic sulfides, Sci. China Chem. 66 (2023) 3290–3296, https://doi.org/10.1007/s11426-023-1644-x.

[58] S. Li, L. Dai, L. Li, A.W. Dong, J.N. Li, X.J. Meng, B. Wang, P.F. Li, Post-oxidation of a fully conjugated benzotrithiophene-based COF for photocatalytic detoxification of a sulfur mustard simulant, J. Mater. Chem. A 10 (2022) 13325–13332, https://doi.org/10.1039/d2ta01864k.

[59] B. Zeng, F.W. Huang, Y.X. Wang, K.H. Xiong, X.J. Lang, TEMPO radically expedites the conversion of sulfides to sulfoxides by pyrene-based metal–organic framework photocatalysis, Chin. J. Catal. 58 (2024) 226–236, https://doi.org/10.1016/S1872-2067(23)64601-7.

[60] F.W. Huang, F.L. Zhang, Y.X. Wang, X.J. Lang, Semiconductor cooperative photocatalysis with TEMPO, Trends Chem. 6 (2024) 115–127, https://doi.org/10.1016/j.trechm.2024.01.002.

[61] Y. Chen, M.J. Xu, J.Y. Wen, Y. Wan, Q.F. Zhao, X. Cao, Y. Ding, Z.L. Wang, H.X. Li, Z.F. Bian, Selective recovery of precious metals through photocatalysis, Nat. Sustainability 4 (2021) 618–626, https://doi.org/10.1038/s41893-021-00697-4.

[62] Y.Z. Liu, Y.J. Wang, H. Li, X.Y. Guan, L.K. Zhu, M. Xue, Y.S. Yan, V. Valtchev, S.L. Qiu, Q.R. Fang, Ambient aqueous-phase synthesis of covalent organic frameworks for degradation of organic pollutants, Chem. Sci. 10 (2019) 10815–10820, https://doi.org/10.1039/c9sc03725j.

[63] Z. Zhang, W.G. Liu, Y.Y. Zhang, J.W. Bai, J. Liu, Bioinspired atomic manganese site accelerates oxo-dehydrogenation of N-heterocycles over a conjugated tri-s-triazine framework, ACS Catal. 11 (2021) 313–322, https://doi.org/10.1021/acscatal.0c04651.

[64] H.J. Shang, Y. Chen, S.H. Guan, Y. Wang, J.Z. Cao, X.R. Wang, H.X. Li, Z.F. Bian, Scalable and selective gold recovery from end-of-life electronics, Nat. Chem. Eng. 1 (2024) 170–179, https://doi.org/10.1038/s44286-023-00026-w.